Science Press

ARTICLE

Evolution and Multistage Regulation of Molten Pool Morphology by Pulsed Laser-Gas Tungsten Arc Hybrid Welding of Magnesium Alloy

Xu Zhen[1,2], Hou Zhonglin[1,2], Zhao Tan[2], Pang Qihang[1,2], Li Shengli[1,2]

[1] School of Materials and Metallurgy, University of Science and Technology Liaoning, Anshan 114051, China; [2] State Key Laboratory of Metal Material for Marine Equipment and Application, Anshan 114009, China

Abstract: With the novel dual heat source model for pulsed laser-gas tungsten arc (GTA) hybrid welding by COMSOL Multiphysics, the temperature distribution was analyzed at several selected points along the weld line. The influences of laser pulse parameters and electric arc current on the welding pool morphology were investigated. The results show that the influence of different process parameters on the depth of molten pool ranked in order is as follows: laser excitation current>arc current>laser pulse width>laser pulse frequency. The influence of different process parameters on the width of molten pool ranked in order is as follows: arc current> laser pulse width or laser excitation current>laser pulse frequency. A database of molten weld pool characteristics for laser-induced arc welding of magnesium alloy was established by classifying the composite heat source parameters and used to realize the precise control of the molten pool shape. The precise control of the actual welding molten pool of a T-shaped weld is achieved with accuracy of 95.1%.

Key words: pulsed laser-gas tungsten arc hybrid welding; pulsed laser parameters; molten pool morphology; multistage regulation

The laser-arc hybrid heat source was first proposed by Ghulam in 1979[1,2], which combines two heat sources of completely different physical properties and heating mechanisms to create a new and more efficient heat source. Integrating heat sources can overcome the disadvantages of individual heat source and result in a synergistic effect[3-5]. The organic combination of two heat sources have the advantages as follows[6-9]: (1) improvement on energy utilization, arc stability, and welding penetration; (2) quality improvement of the workpiece surface with reduced tooling accuracy; (3) improved welding efficiency and reduced cost; (4) improved weld shape with less welding defects.

The laser-arc composite heat source has been extensively researched owing to the broad application prospects. Li et al[10] showed that cold filler wire improves the weld performance in low-power laser-gas tungsten arc (GTA) welding of T-shaped joints of magnesium alloy. The optimal weld surface and weld pool formation were obtained with a laser power of 300 W, welding speed of 1000 mm/s, and arc current of 100 A. Mahrle et al[11] introduced a low-power laser to effectively restrain the arc current fluctuations, thereby obtaining the stable electric arc. Chen et al[12] studied the relationship between keyhole stability and welding porosity in laser-gas tungsten arc (GTA) welding of magnesium alloy. Pores are generally located at the bottom of fusion zone of the joint. Therefore, a higher aspect ratio increases the rate of pore formation, whereas the overlap of adjacent laser keyholes effectively reduces porosity.

Advanced computing and numerical analysis methods have become powerful tools for studying welding technology. In recent years, a large number of researches have been conducted on laser-arc composite welding using computer simulations[13-15]. Gao et al[16] simulated the morphology and size of the weld pool generated by composite heat source under

different process conditions. As the arc current increases, the radii of molten pool and curvature of the fusion line in the small hole area increase. Moreover, when the arc current is stable, the radius of curvature gradually increases and becomes deeper and narrower as the laser power increases. Akbari et al[17] used bulk heat sources instead of surface heat sources to simulate the laser welding process of titanium alloy Ti6Al4V, and reduced the error between the size of simulated molten pool and tested molten pool to 2%~7%. Temperature changes abruptly near the center of the laser beam, and shows that the farther from the laser loading position, the smaller the temperature gradient. Faraji et al[18] proposed a three-dimensional numerical model based on the finite element volume method and performed simulations to study the heat transfer and fluid flow behavior during the laser-TIG arc welding process. The geometry of the molten pool is determined by analyzing the welding performance of AA6082 aluminum alloy. Several dimensionless numbers are derived to distinguish the importance of various forces driving fluid flow in the welded molten pool. Hou[19] used the extended application of COMSOL Multiphysics to establish a novel dual heat source model for pulsed laser-GTA hybrid welding. The model successfully solved the inaccuracy problem of simulation caused by the energy superposition effect owing to the distinct physical characteristics of the laser and arc.

In this study, the extended application of COMSOL Multiphysics was used to establish a database of molten pool morphologies obtained by laser induced arc welding of magnesium alloy. The database was then used to investigate the effects of various welding process parameters on the weld pool morphology. Precise control of molten pool morphology by low-power laser-GTA welding can be achieved through graded adjustment of the compound heat source parameters. Finally, a real welding experiment using a complex T-shaped part was conducted to verify the accuracy and applicability of this method.

1 Experiment

The composition of magnesium alloy AZ31B is presented in Table 1. The thermodynamic parameters used in simulations are listed in Table 2. The specific heat coefficient and heat conduction coefficient were specified in the COMSOL Multiphysics software. Latent heat was taken as the equivalent specific heat in all simulations.

By combining the GTA heat source model with the laser

heat source model, a novel dual heat source model was acquired as the hybrid heat source, and could be expressed by Eq.(1) and Eq.(2), as follows[19-21]:

$$q_{GTA}(x,y,t) = \frac{3Q_1}{\pi r_0^2} \exp \left\{ -\frac{3[x^2 + (y - v_0 t)^2]}{r_0^2} \right\} \quad (1)$$

where q_{GTA} is the heat flux of the GTA; Q_1 is the GTA power, with $Q_1 = U_1 I_1 g_1$, in which U_1, I_1, and g_1 are the arc voltage, current, and heat efficiency, respectively; r_0 is the effective radius of the arc heat source; v_0 is welding speed; t is welding time; x and y are coordinates on the x and y axes, respectively.

$$q_{laser}(x,y,z,t) = \frac{9Q_2 \eta_2}{\pi R_0^2 H (1-\frac{1}{e^3})} \exp \left\{ -\frac{9[x^2+(y-v_0 t)^2]}{R_0^2 \ln (\frac{H}{z})} \right\} \quad (2)$$

where q_{laser} is the heat flux of the laser; R_0 is the laser beam radius; H is the height of the heat source; η_2 is the laser heat source efficiency; Q_2 is the pulsed laser power output; z is the z-axis coordinate.

The pulse laser-induced arc composite welding process involves rapid heating and air cooling. The temperature distribution is unstable and varies along different coordinate directions. The temperature T during the welding process can be expressed as follows:

$$\rho c \frac{\partial T}{\partial t} = \frac{\partial}{\partial x} \left(k \frac{\partial T}{\partial x} \right) + \frac{\partial}{\partial y} \left(k \frac{\partial T}{\partial y} \right) + \frac{\partial}{\partial z} \left(k \frac{\partial T}{\partial z} \right) + L_m + Q_a \quad (3)$$

where ρ is density, c is specific heat capacity, k is thermal conductivity, L_m is latent heat of fusion, and Q_a is the energy density of the internal heat source, which is expressed as follows:

$$Q_a = q_{GTA} + q_{laser} \quad (4)$$

Heat transfer through convection and radiation from the workpiece to the environment is complex. To simplify the calculation, a specific heat transfer coefficient of 12 W·m^{-2}·K^{-1} was applied and the initial temperature of the workpiece was 293 K.

A numerical simulation model of the bead-on-plate welding process of magnesium alloy AZ31B was established in the COMSOL Multiphysics software. The size of the specimen plate was 100 mm×50 mm×6 mm, as shown in Fig. 1. The plate was geometrically symmetrical and the plate was also symmetrically loaded. Therefore, only half of the plate was considered. As illustrated in Fig.1, a free-cut tetrahedral mesh with a minimum size of 0.05 mm was applied in the welding zone, a refined mesh with 300 constant units was used at the weld bead boundary, and an intelligence-dealt mesh was applied far away from the weld bead. Values of laser (LWS-1000) and GTA (OTC-500) parameters used in the experiment are presented in Table 3.

After the experiment of laser induced arc composite T-joint welding was conducted, a wire cutting machine was used to cut specimens at certain positions along the welded joint, and

Table 1 Chemical composition of magnesium alloy AZ31B (wt%)

Al	Zn	Mn	Si	Cu	Mg
2.5~3.5	0.7~1.3	0.2~1.0	<0.05	<0.01	Bal.

Table 2 Physical property parameters of magnesium alloy AZ31B

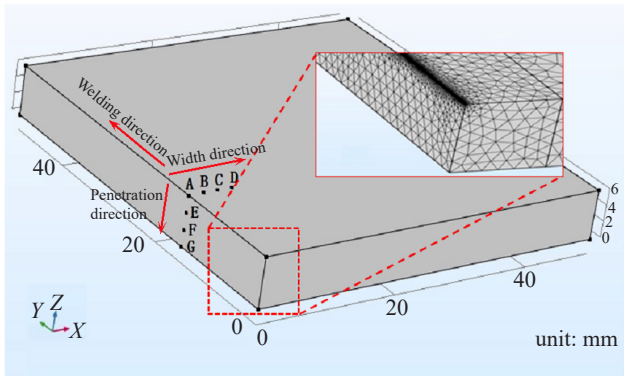| Melting point/ °C	Boiling point/ °C	Latent heat of fusion/ kJ·kg^{-1}	Latent heat of vaporization/ kJ·kg^{-1}	Specific heat/ kJ·kg^{-1}·K^{-1}	First ionization energy/ kJ·mol^{-1}
935±5	1390	360~377	6113~6238	1.025	116

Fig.1   Schematic diagram of weld model and selected points for COMSOL simulations

the specimens were then prepared by mechanically polishing. Finally, specimens were corroded with the corrosive agent (5 mL acetic acid+5 g picric acid+100 mL alcohol+10 mL water), cleaned in alcohol and dried, and then observed under an Leica DMI5000M optical metallurgical microscope.

2 Results and Discussion

2.1 Temperature distribution characteristics of weld seam under different process parameters

Process parameters affect the temperature distribution essentially during welding. Therefore, this study focuses on

thermal cycle curves at different positions along the weld seam. The effect of laser pulse parameters and arc current on the temperature field is quantitatively assessed. As shown in Fig. 1, the point coordinates selected in the geometric model for COMSOL simulations are: point A (0, 15, 6) at the edge; point B (2, 15, 6), point C (4, 15, 6), and point D (6, 15, 6) along the width direction of the weld cross section; point E (0, 15, 4), F (0, 15, 2), and G (0, 15, 0) along the penetration direction of the weld.

Fig. 2a and 2b show the thermal cycle curves at different points along the width and penetration directions with a laser pulse of 150 A, pulse of 3 ms, pulse frequency of 25 Hz, arc current of 125 A, and welding speed of 10 mm/s, respectively. As the laser-arc composite heat source continues to approach the point D and G along the width and penetration directions, respectively, the average and maximum temperatures at each location are lower with the heat source moving away. In addition, the heating and cooling rates are slower and the residence time above the melting temperature is shorter. When the composite heat source is close to selected points, the thermal cycle curves of point A, E, F, and G in Fig.2b indicate a sharp temperature rise and fall due to the multiple pulsed lasers with a high peak power output applied periodically, causing a sharp change in temperature at these locations. Besides, the short interval between two adjacent laser pulses indicates that the heat generated by the previous pulse is not fully diffused before the next pulse, and the heat from the previous pulse period is retained. Therefore, the heat from

Table 3 Critical thermal parameters along welding width and penetration directions under different process conditions

| Thermal parameter		Point	Excitation current/A		Pulse width/ms		Pulse frequency/Hz		Arc current/A	
			100	200	2	5	5	25	75	150
Width direction	Maximum temperature/K	A	1505	2650	1785	2030	1690	1750	1850	2425
		B	1005	1095	985	1205	985	1025	965	1250
		C	780	845	770	830	770	795	720	950
		D	630	680	615	690	625	645	590	750
	Average temperature increment/K		215		391		28		543	
	Residence time above melting point/s	A	0.50	1.05	0.65	0.85	0.61	0.62	0.45	1.10
		B	0.21	0.32	0.25	0.33	0.24	0.24	0.20	0.68
		C	0	0	0	0	0	0	0	0
		D	0	0	0	0	0	0	0	0
	Average increment of residence time/s		0.10		0.19		0		0.41	
Penetration direction	Maximum temperature/K	A	1405	2450	1785	2030	1590	1650	1850	2425
		E	1190	1810	1260	1335	1300	1350	1050	1420
		F	950	1350	985	1065	1050	1075	825	1085
		G	620	810	680	765	645	665	645	755
	Average temperature increment/K		790		185		25		455	
	Residence time above melting point/s	A	0.50	1.05	0.65	0.85	0.61	0.62	0.45	1.10
		E	0.32	0.81	0.39	0.42	0.41	0.42	0.21	0.62
		F	0.05	0.24	0.07	0.09	0.1	0.1	0.04	0.10
		G	0	0	0	0	0	0	0	0
	Average increment of residence time/s		0.45		0.11		0		0.33	
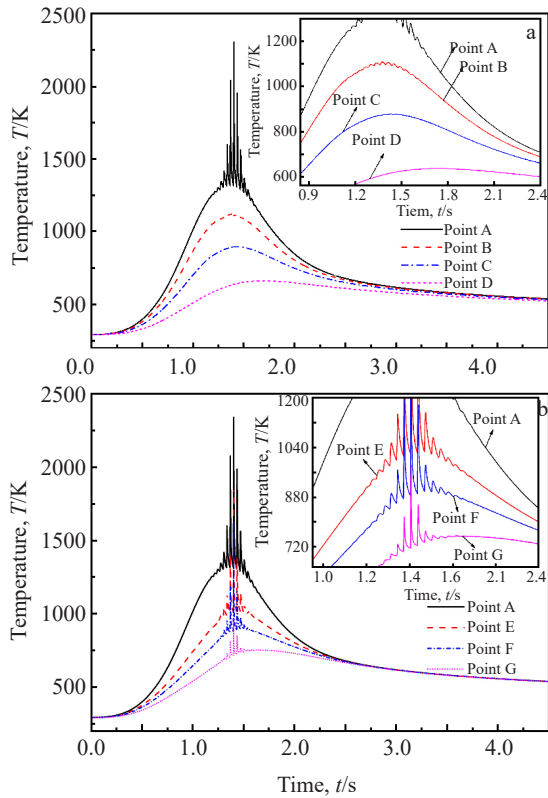
Fig.2 Thermal cycle curves at different location points along width (a) and penetration (b) directions

each cycle accumulates. As a result, the temperature continues to increase at this location. The thermal cycle curves of point B and C (Fig. 2a) exhibit heat accumulation with a lower extent, which suggests that each point along the penetration direction is subjected to the heat accumulation effect due to the thermal effects of pulse energy of the composite heat source. Along the width direction, the heat accumulation phenomenon weakens as the length from the center of the laser action increases.

Under these conditions, the critical thermal parameters along width and penetration directions are obtained through finite element simulations in COMSOL, as shown in Table 3. When the laser excitation current increases from 100 A to 200 A with other fixed process parameters, the maximum temperature at each point along the penetration direction significantly increases. The average temperature increment is 790 K, representing an increase of 49%. The average residence time at temperatures above the melting point increases by 43% with the increment of 0.45 s. The increase in maximum temperature along the width direction of the molten pool is lower. The average increment in temperature is 215 K, increasing by 20.5%. The average residence time at temperatures above the melting point increases by 18% with the increment of 0.10 s. This is because the pulsed laser heat source transfers bulk heat. Therefore, as the laser excitation current increases, the peak power during the pulse action and heat flux density of the laser heat source increase considerably

along the penetration direction of the molten pool, thereby significantly increasing the temperature along the penetration direction. Similarly, as the laser pulse width increases, the heat input duration along the penetration and width directions of the molten pool increases, resulting in an increase in the temperature of the molten pool area. However, the increase in maximum temperature along the penetration direction is less obvious than that along width direction. The change in pulse frequency has little effect on temperature parameters along the penetration and width directions and can be ignored. As the arc current increases, the maximum temperature, average temperature increment, and the residence time of temperature above the melting point along the penetration and width directions significantly increase.

In summary, the quantitative results describing the influence of four parameters of the composite heat source on the temperature distribution of the weld are obtained. The composite heat source parameters are ranked in order according to their influence on temperature along the penetration direction of the molten pool: laser excitation current (primary influence) ＞arc current (secondary influence) ＞laser pulse width (weak influence) ＞laser pulse frequency (negligible influence). The influence of parameters on temperature along the width of the molten pool is ranked in order, as follows: arc current (primary influence) ＞laser pulse width or laser excitation current (weak influence) ＞laser pulse frequency (negligible influence).

2.2 Database-based control method of molten pool morphology

Fig. 3 presents a typical nail-shaped molten pool morphology of laser induced arc welding. To precisely characterize the shape of the molten pool, such as nail cap width, nail cap thickness, nail head length, and nail head waist width, three sets of simulated process parameters were designed: (1) a pulse excitation current of 125 A, pulse width of 3 ms, pulse frequency of 20 Hz, and arc current of 70~150 A; (2) a pulse excitation current of 100~200 A, pulse width of 3 ms, pulse frequency of 20 Hz, and arc current of 125 A; (3) a pulse excitation current of 125 A, pulse width of 2~5 ms, pulse frequency of 20 Hz, and arc current of 125 A. According to the reported literature, a laser pulse with frequency higher than 20 Hz can realize continuous welding of longitudinal sections[20]. To reduce energy consumption, the pulse frequency in each process is 20 Hz.
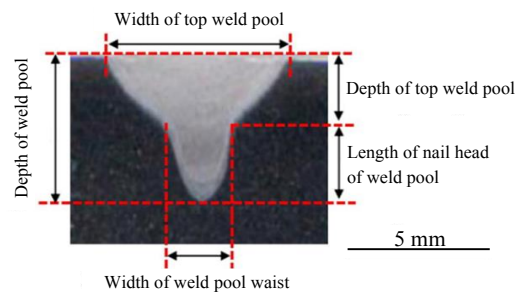

Fig.3 Morphology of weld pool by laser-arc hybrid welding of magnesium alloy AZ31B

Fig. 4 shows that within the laser induced arc welding parameter range, the melting width of the nail cap surface of the molten pool and the thickness of the nail cap change significantly as the arc current parameter varies. The arc current is the main heat output of the compound heat source and controls the depth and width of the molten pool. It is therefore the main influence factor on molten pool morphology. The laser excitation current variation changes the length and top width of the nail head of molten pool nail hole. The length of nail head extends from 3.3 mm to 6.1 mm, which controls the shape of the nail head at the bottom of the molten pool. The laser excitation current is the secondary influencing factor for the morphology of molten pool. Changes in the laser pulse parameter only have a small effect on the width of the top of weld nail cap and the width of nail head waist, making the laser pulse a weak influence factor.

Based on the analysis, a database of weld pool parameters was constructed for heat source parameters within a fixed parameter range (laser excitation current of 100~200 A, laser pulse width of 2~5 ms, pulse frequency of 20 Hz, and arc current of 75~150 A). The arc current, laser excitation current, and laser pulse width are the first-level, second-level, and third-level datasets, which are selected as 5 A, 5 A, and 0.5 ms, respectively. The first-level dataset is used to construct an arc current system according to an incremental increase (ΔI_1) in arc current, as shown in Fig. 5a. The second-level dataset refers to any arc current system in the first-level dataset, and the parameter range of the laser excitation current can be built into m sets of excitation current systems according to a certain incremental increase (ΔI_2), as shown in Fig. 5b. The third-level dataset refers to any laser excitation current system in the second-level dataset. The laser pulse width parameter range can be constructed according to a certain incremental decrease (Δt_p) to form a single-group pulse width system, as shown in Fig.5c.
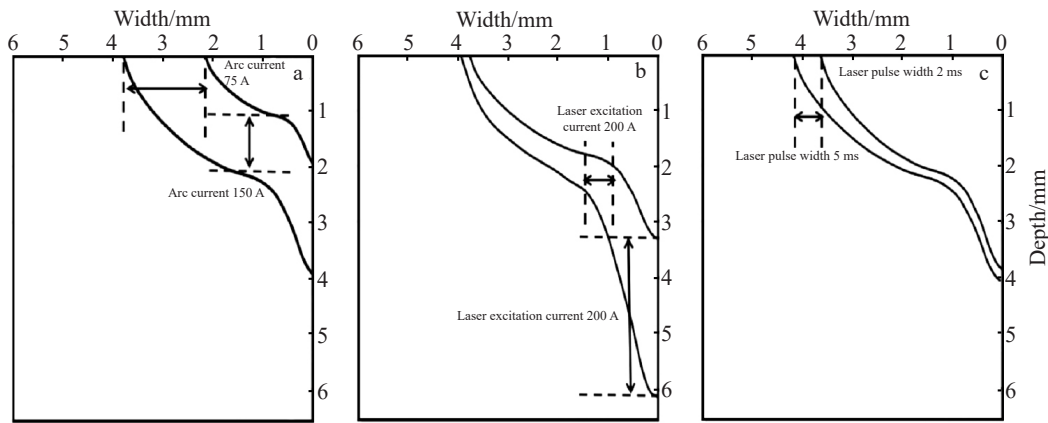

Fig.4   Influences of arc current (a), laser excitation current (b), and laser pulse width (c) on cross-sectional morphologies of magnesium alloy AZ31B by laser-arc hybrid welding
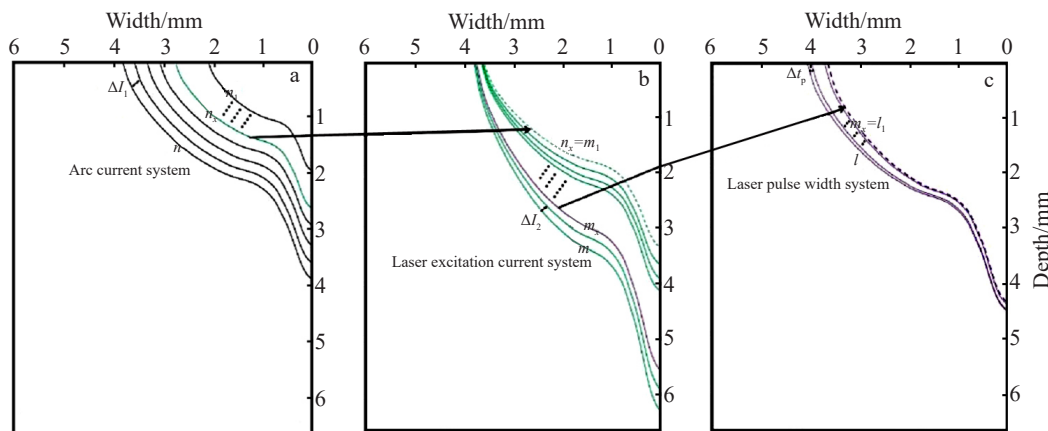

Fig.5   Three-level systems for database construction of weld pool shape: (a) arc current system; (b) laser excitation current system; (c) laser pulse width system

The database of molten pool morphology of magnesium alloy AZ31B by laser induced arc welding has two main functions: (1) to accurately predict the weld pool shape and size based on the process parameters of the composite heat source; (2) to accurately regulate and control the arc current, laser excitation current, and pulse width parameters based on the size of workpiece and the joint mode for laser-arc hybrid welding of magnesium alloy AZ31B.

Take the precise control of the molten pool morphology in butt welding of magnesium alloy flat plate with thickness of Z mm as an example. In this case, the specific steps of the method are as follows.

Step 1: Determine the critical parameters of the molten pool in flat butt welding. According to the thickness of the plate, the basic melting depth is Z mm. The penetration refers to the width at the back of the molten pool (d_u) and is a key parameter in flat butt welding. The back weld pool width threshold is Y mm and determined according to the welding manual and actual butt welding of plate of thickness of Z mm.

Step 2: Initial adjustment. Take the minimum value of the laser excitation current and laser pulse width as fixed parameters. Extract the corresponding 16 sets of arc current system from the first-level dataset, as shown in Fig.6a. When the melting depth of the base is Z mm and the intersection point of the straight line of the back weld pool width and longitudinal axis is above point B, the nearest arc current system of n_x A is selected.

Step 3: First fine tuning. Select 21 sets of laser excitation current system parameters corresponding to the arc current of n_x A from the second-level dataset, as shown in Fig.6b. Select the laser excitation current m_x A corresponding to the preset weld width at the back of weld pool (BE is the width at the back of weld pool, and its value is $Y/2$ mm in Fig. 6b). The selected process follows the principle that if an intersection (point B or E in Fig.6) exists between the straight line of the back weld pool width and laser excitation system, the closest laser excitation system of m_x A to the right of the intersection is selected. If there is no intersection point, it is necessary to increase the level of the first arc current system to n_{x+1} A until

the straight line of the back weld pool width intersects with the laser excitation system.

Step 4: Final fine tuning. In the third-level dataset, 7 sets of laser pulse width systems corresponding to the arc current of n_x A and an excitation current of m_x A are extracted, as shown in Fig.6c. The excitation current of l_x ms corresponding to the preset weld width at the back of the weld pool (BE=$Y/2$ mm in Fig. 6c) is selected. If an intersection exists between the straight line of the back weld pool width and each pulse width system, the laser pulse width system of l_x ms with the closest intersection is selected. If there is no intersection, it is necessary to increase the current level of the m_{x+1} A until the straight line of the back weld pool width intersects with the laser pulse width system and the laser pulse width system can be determined. The above steps can identify the suitable control parameters for weld pool morphology of magnesium alloy AZ31B with thickness of Z mm by butt welding, including the arc current n_x A, laser excitation current m_x A, and laser pulse width l_x ms.

2.3 Application of weld pool shape control of T-shaped joint

Laser-arc composite heat source welding offers advantages of deep penetration ability, small welding deformation, and low energy consumption, and can realize unilateral welding of the wall plate of T-shaped structural parts. However, if the process parameters for the composite heat source are not suitable, the welding failure occurs. For example, when the laser excitation current is too small, the penetration capacity is not sufficient and only the upper part of the wall plate of the T-shaped weldment melts. Since the lower part of the rib plate does not melt, the connection between the wall plate and the rib plate cannot be realized, as shown in Fig.7a. When the arc current is too large, the molten pool is large, and the liquid metal remains at high temperature for a long time, making it difficult for the surface tension of the molten pool to support a large amount of liquid metal due to gravity, and burn-through defects eventually appear, as shown in Fig.7b. In addition, for single-side welding of T-shaped parts, it is necessary to select a suitable back width of the wall plate, which allows a
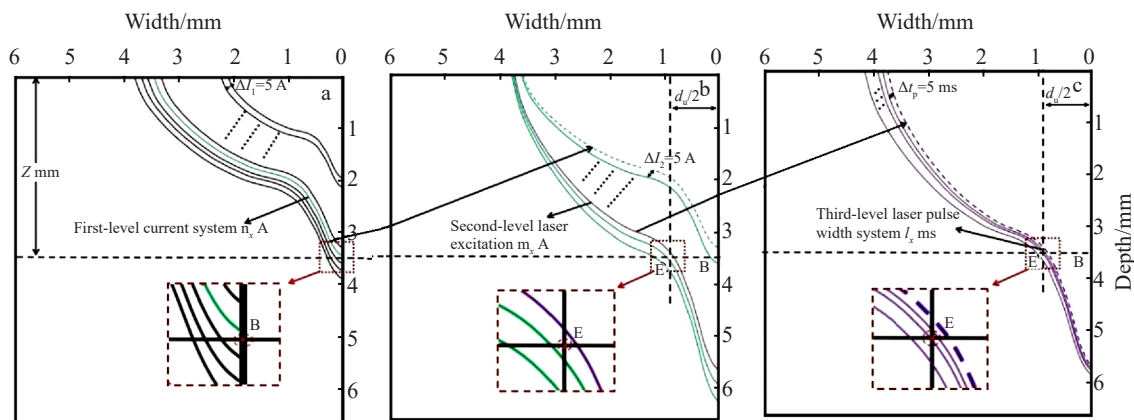

Fig.6   Weld pool shape control processes in butt welding: (a) initial adjustment; (b) first fine tuning; (c) final fine tuning
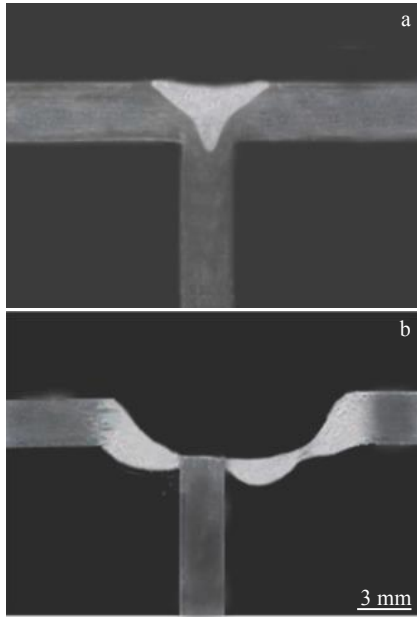
Fig.7   Weld morphologies of T-shaped joint by laser-arc welding:
(a) unfused and (b) excessive melting

uniform transition weld to form on both sides of the weld back between the rib plate and the wall plate, avoiding stress concentration and increasing the strength of the weldment. Adjusting process parameters of the composite heat source and controlling the weld pool morphology ensure the weld quality in laser-arc composite welding of T-shaped parts.

In this research, T-shaped magnesium alloy parts with a wall and rib thickness of 2.5 mm were used for calculations. The welding method is one-sided welding. The process for controlling molten pool morphology based on the magnesium alloy composite welding database is as follows. The melting depth is determined as 2.5 mm based on the thickness of the rib and wall plates. To address the problems of laser arc welding of T-shaped magnesium alloy parts, the formation of a certain width of transition weld (d_L) and the melt width (d_u) on the back of wallboard are taken as the critical parameters of the molten pool, according to the requirements of the welding manual for the geometric design of a T-shaped one-sided weld joint and actual results of the welding experiment. d_L is set as 1 mm, which is two fifths of the thickness of the rib plate. Then, the back melting width/2=d_L+rib thickness= 2.25 mm, as shown in Fig.8.

The minimum laser excitation current and pulse width range are fixed parameters from the first-level dataset and the corresponding arc current system is extracted. An arc current of 115 A is selected, corresponding to a melting depth of 2.5 mm. Again, the laser excitation system is extracted from the second-level dataset corresponding to an arc current of 115 A. The line corresponding to the melt width (BE=2.25 mm) on the back of the molten pool does not intersect with the laser excitation system line. By increasing the level of the first-
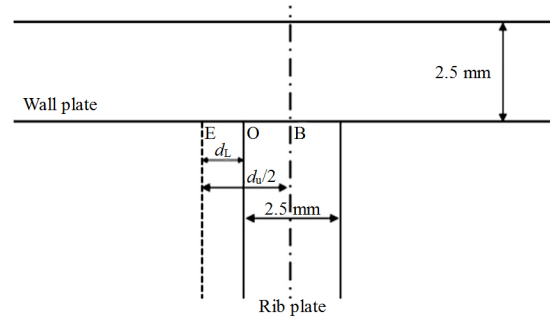

Fig.8   Schematic diagram of welded T-shaped joint

level arc current system twice, the arc current system is determined to be 125 A and the laser excitation current is 145 A. Finally, 7 groups of laser pulse width system corresponding to arc current of 125 A and laser excitation current of 145 A are extracted from the third-level dataset, and the laser pulse width is determined to be 3.5 ms, thereby realizing fine adjustment of the melting width of the wall back of the molten pool.

Then the parameters for the welding pool of T-shaped magnesium alloy part with thickness of 2.5 mm are: arc current of 125 A, laser excitation current of 145 A, and laser pulse width of 3.5 ms. The final system diagram and simulated morphology obtained from the control process are shown in Fig. 9. Fig. 9b shows the cross-sectional morphology of weld pool. The actual melt pool morphology is in good agreement with
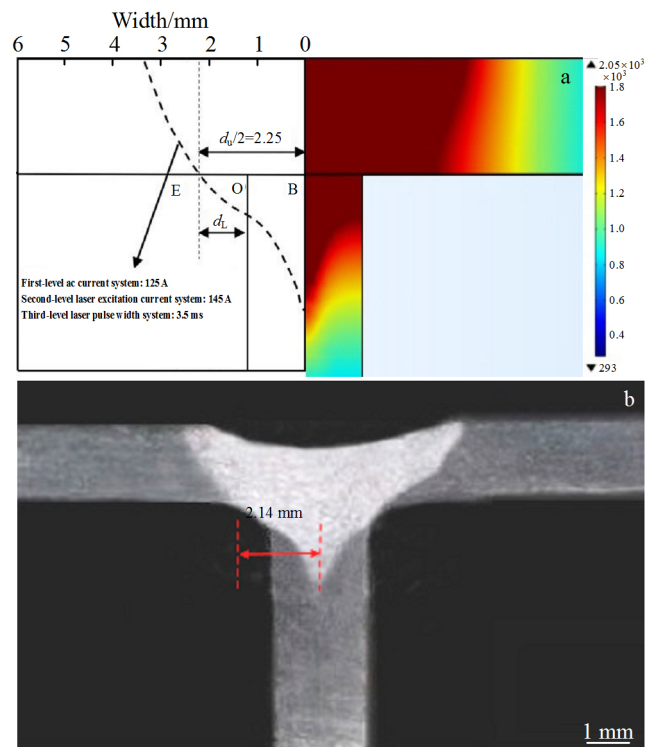

Fig.9   Simulated molten weld shape of T-shaped joint (a); actual cross-sectional morphology of T-shaped joint weld pool (b)

the simulated melt pool line (the degree of coincidence is about 95.1%), which suggests that the molten pool control method based on the database system is highly accurate.

3 Conclusions

1) The temperature at different points in the weld pool rapidly increases and decreases periodically due to the thermal effects of the composite heat source of the arc plasma induced by the pulse laser. Multiple pulse cycles result in heat accumulation effects, which influences the depth of weld pool.

2) The influence of different parameters of the composite heat source on the temperature distribution of the weld is quantified. The composite heat source parameters are ranked in order according to their influence on temperature along the penetration direction of the molten pool: laser excitation current (primary influence)＞arc current (secondary influence)＞laser pulse width (weak influence) ＞laser pulse frequency (negligible influence). The influence of parameters on temperature along the width of the molten pool is ranked in order, as follows: arc current (primary influence)＞laser pulse width or laser excitation current (weak influence)＞laser pulse frequency (negligible influence).

3) A database is constructed for developing a method for controlling the molten pool shape of magnesium alloy by laser-arc hybrid welding based on initial adjustment of the first-level arc current system, fine adjustment of the second-level laser excited current system, and fine adjustment of the third-level laser pulse width system. Precise control of the weld pool of a complex T-shaped welding joint with an accuracy of 95.1% is obtained.

References

1 Bagger C, Olsen F O. *Journal of Laser Applications*[J], 2005, 17(1): 2

2 Guo Yuquan, Wu Dongjiang, Ma Guangyi *et al. Rare Metal Materials and Engineering*[J], 2014, 43(11): 2663

3 Yang Qingshan, Jiang Bing, Xiang Qing *et al. Rare Metal Materials & Engineering*[J], 2016, 45(7): 1674

4 Gao Ming, Mei Shuwen, Wang Zemin *et al. Journal of Materials Processing Technology*[J], 2012, 212(6): 1338

5 Guan Z S, Wang W X, Cui Z Q *et al. Rare Metal Materials and Engineering*[J], 2015, 44(7): 1597

6 Shinn B W, Farson D F, Denney P E. *Science and Technology of Welding and Joining*[J], 2013, 10(4): 475

7 Tan Hua, Chen Jing, Zhang Fengying *et al. Rare Metal Materials and Engineering*[J], 2009, 38(4): 574

8 Roepke C, Liu S, Kelly S. *Welding Journal*[J], 2010, 89(7): 140

9 Yan J, Gao M, Zeng X Y. *Optics and Lasers in Engineering*[J], 2010, 48(4): 512

10 Li C B, Liu L M. *The International Journal of Advanced Manufacturing Technology*[J], 2013, 65(1-4): 27

11 Mahrle A, Rose S, Schnick M *et al. Science and Technology of Welding and Joining*[J], 2013, 18(4): 323

12 Chen M H, Xu J N, Xin L J *et al. Optics and Lasers in Engineering*[J], 2017, 93: 139

13 Li Z Y, Wei X T, Sun J J *et al. The International Journal of Advanced Manufacturing Technology*[J], 2016, 85(9): 2557

14 Wu Q, Xue N P, Zhang Y D *et al. The International Journal of Advanced Manufacturing Technology*[J], 2020, 107(3): 1671

15 Shen X, Gao K, Dong S. *The International Journal of Advanced Manufacturing Technology*[J], 2020, 107(9): 3953

16 Gao Z G, Ojo O A. *Acta Materialia*[J], 2012, 60(6-7): 3153

17 Akbari M, Saedodin S, Toghraie D *et al. Optics & Laser Technology*[J], 2014, 59: 52

18 Faraji H A, Goodarzi M. *The International Journal of Advanced Manufacturing Technology*[J], 2015, 77(9): 2067

19 Hou Z L, Liu L M, Lv X Z *et al. Journal of Iron and Steel Research International*[J], 2018, 25(9): 995

20 Zhang Yingming, Zhou Lian, Sun Jun *et al. Rare Metal Materials and Engineering*[J], 2008, 37(11): 1973

21 Liu Chuan, Zhang Jianxun, Niu Jing *et al. Rare Metal Materials and Engineering*[J], 2009, 38(8): 1317

镁合金低脉冲激光-气体混合焊的熔池形貌演变和多级调控

徐　振[1,2]，侯忠霖[1,2]，赵　坦[2]，庞启航[1,2]，李胜利[1,2]

(1. 辽宁科技大学 材料与冶金学院，辽宁 鞍山　114051)

(2. 海洋装备用金属材料及其应用国家重点实验室，辽宁 鞍山　114009)

摘　要：利用基于COMSOL Multiphysics的脉冲激光-气体钨极电弧（GTA）混合焊接新型双热源模型，分析了焊缝沿线选定点的温度分布，研究了激光脉冲参数和电弧电流对熔池形貌的影响。工艺参数对熔池深度的影响由大到小为：激光激励电流＞电弧电流＞激光脉冲宽度＞激光脉冲频率；工艺参数对熔池宽度的影响由大到小为：电弧电流＞激光脉冲宽度或激光激励电流＞激光脉冲频率。在此基础上，构建了激光诱导电弧焊接镁合金熔池形貌数据库体系，通过复合热源参数的分级调控，以实现对熔池形貌的精准控制。利用T形焊接熔池来验证熔池形貌的调控效果，结果表明控形的准确度高至95.1%。

关键词：脉冲激光-气体混合焊；脉冲激光参数；熔池形貌；多级调控

作者简介：徐　振，男，1987年生，博士，讲师，辽宁科技大学材料与冶金学院，辽宁 鞍山　114051，电话：0412-5929529，E-mail：xuzhen_ustl@sina.com